Discover Water

Brief Communication

A link between the global surface area receiving daily precipitation, wet-day frequency and probability of extreme rainfall

Rasmus E. Benestad[1] · **Cristian Lussana**[1] · **Andreas Dobler**[1]

Received: 24 July 2023 / Accepted: 19 February 2024
Published online: 04 March 2024

Abstract
Both the total amount of precipitation falling on Earth's surface and the fraction of the surface area on which it falls represent two key global climate indicators for Earth's global hydrological cycle. We show that the fraction of Earth's surface area receiving daily precipitation is closely connected to the global statistics of local wet-day frequency and mean precipitation intensity, based on the ERA5 reanalysis. Our analysis of the global statistical distribution of local temporal mean precipitation intensity μ revealed a close link between (1) its global spatial average $\langle\mu\rangle$ and (2) the total daily precipitation falling on Earth's surface divided by the global surface area fraction on which it falls. This correlation highlights an important connection, since the wet-day frequency and the mean precipitation intensity represent two key parameters that may be used to approximately infer the probability of heavy rainfall on local scales. We also found a close match between the global mean surface temperature and both the total mass of 24-h precipitation falling on Earth's surface as well as surface area receiving 24-h precipitation in the ERA5 data, highlighting the dependency between the greenhouse effect and the global hydrological cycle. Moreover, the total planetary precipitation and the daily precipitation area represent links between the global warming and extreme precipitation amounts that traditionally have not been included in sets of essential climate indicators. A simple back-of-the-envelope calculation suggests that half of $\Delta\langle\mu\rangle/\Delta T = 0.47$ mm/day can be explained by increased 24-h precipitation and half by a reduced fractional area of 24-h precipitation.

Keywords Global hydrological cycle · Precipitation surface area · Mean precipitation intensity · Extreme precipitation

1 Introduction

Global warming caused by the strengthening of the greenhouse effect is expected to lead to more extreme weather events [1, 2], and one explanation for more extreme rainfall is that higher temperatures near Earth's surface and in the air favour higher rates of evaporation and an increase in the moisture holding capacity of the air according to the Clausius–Clapeyron equation [3, 4]. We can refer to the connection between water vapour and temperature as the '*thermodynamic effect*' of climate on the hydrological cycle.

Supplementary Information The online version contains supplementary material available at https://doi.org/10.1007/s43832-024-00063-3.

✉ Rasmus E. Benestad, rasmus.benestad@met.no; Cristian Lussana, cristian.lussana@met.no; Andreas Dobler, andreas.dobler@met.no | [1]The Norwegian Meteorological Institute, Henrik Mohns plass 1, Oslo 0313, Norway.

Allan et al. provides a comprehensive literature review on the status of current knowledge regarding precipitation and hydrology [5], and an additional overview is provided in the sixth assessment report from the Intergovernmental Panel on Climate Change [2]. Both give an account of an increasingly detailed picture with advanced levels of complex interactions. However, neither discuss the fraction of Earth's surface receiving precipitation on a daily basis, although they do delve into fast adjustments that scale with radiative forcing and slow temperature-driven responses to radiative forcing. Here we take a more heuristic approach in order to unveil how global physical aspects, such as the fraction of Earth's surface receiving 24-h precipitation and the total global 24-h precipitation, are linked to both global warming and rainfall pattern characteristics.

Increased concentrations of greenhouse gases inhibit the transmission of longwave radiation from the planetary surface, a branch of the energy flow from Earth's surface to the top of the atmosphere. An increased constraint in the vertical radiative energy flow may result in an increased atmospheric overturning rate with an increased latent heat flow through deep convection to compensate for the reduced radiative energy flow. The latent heat transport connects the energy flow and the circulation of H_2O (water, vapour, ice), and in a long-term steady-state global hydrological cycle, the total mass of water evaporated (E) in a closed system, such as Earth's climate system, equals the total global precipitation (P) when integrated over the Earth's surface area ($A \approx 4\pi r_e^2$, where $r_e = 6371$ km is Earth's radius). We use the upper-case notation P for global spatial statistics and lower-case p for local data (i.e. grid point values), moreover the notation $\langle \cdot \rangle$ stands for the spatial average, while $\bar{\cdot}$ is for the temporal average. Then, we can write $E = \int_A e \, dA$ and $P = \int_A p \, dA$, such that $\overline{E} = -\overline{P}$ over a sufficiently long time period when Earth's global hydrological cycle is in a steady state. However, neither evaporation nor precipitation are uniform in time or space, and evaporation takes place over a different planetary surface area (A_e) than the surface area on which precipitation falls on a daily basis (A_p). For instance, evaporation takes place continuously over wet surfaces such as the world oceans (cover about 70% of Earth's surface area), albeit with a dependence on temperature and wind. In contrast, it doesn't rain everywhere or all the time. We use the expression $A'_p = A_p/A$ to denote the fraction of the global surface area receiving 24-h precipitation.

In previous studies it has been assumed that a decrease in the precipitation area A_p can explain more extreme daily rainfall amounts and reduced frequency of wet days (f_w) [6], but this has to the best of our knowledge not yet been demonstrated through the analysis of observational data or reanalyses. The connection between a global index, such as A'_p, and local rainfall statistics is expected to involve the global average of the mean precipitation intensity $\langle \mu \rangle$ estimated for all grid-boxes. Moreover, a shift in the global statistical distribution is expected to be linked to the changes in local precipitation intensities μ around the globe. Here, the global mean precipitation intensity $\langle \mu \rangle$ should be interpreted as a parameter describing the statistical distribution of local μ, and we can expect the entire distribution to shift to greater values with an increase in $\langle \mu \rangle$.

Both the local precipitation intensity μ and wet-day frequency f_w appear to be two key parameters when it comes to estimating the probability of local precipitation amount above a given threshold level x [7]:

$$Pr(X > x) \approx f_w \exp\left(-\frac{x}{\mu}\right). \tag{1}$$

This simplified expression describes an approximated estimate for the probability of 24-h precipitation above a threshold x, based on data from 9817 daily rain gauge records world-wide [7]. It provides a rule-of-thumb for moderately high magnitudes, but not for the most extreme cases far out in the tails of the distribution. If the local μ increases as a result of a change in $\langle \mu \rangle$ and a corresponding shift in its spatial statistical distribution, then the probability for heavy rainfall also increases, all else being equal. If we can find a direct connection between the fractional surface with 24-h precipitation A'_p and total global precipitation P, as well as between global mean precipitation intensity $\langle \mu \rangle$ and wet-day frequency $\langle f_w \rangle$, we can then derive generalized rule-of-thumb statements. These would explain the combined impact on both the fractional surface area receiving daily precipitation and total global daily precipitation on the global statistics for local extreme rainfall events. Our objective is therefore to test the assumption that a reduced fractional area with daily rainfall A'_p can be linked to reduced wet-day frequency statistics $\langle f_w \rangle$ and increased mean precipitation intensity statistics $\langle \mu \rangle$. We also briefly examine the connection between the global mean temperature anomaly T and A'_p as well as P.

2 Results

Figure 1 shows that there is a perfect match between the global mean of the annual wet-day frequency and the annual mean of the daily surface area fraction with precipitation if we take into account how the surface area of the grid-boxes vary with latitude, hence $\langle f_w \rangle = \overline{A'_p}$. These two quantities were estimated through different approaches

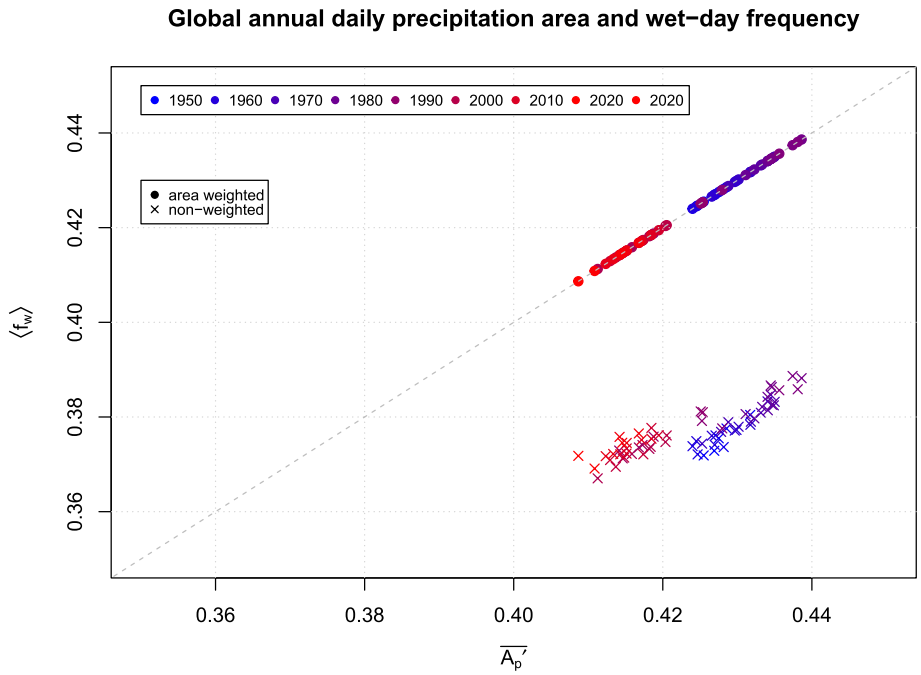

Fig. 1 The global annual mean wet-day frequencies estimated over the days of each year for all ERA5 area-weighted grid-boxes $\langle f_w \rangle$ (circles) show a perfect match with the annual mean fractional surface area with daily precipitation, here shown as $\overline{A'_p}$. The same analysis reveals some discrepancies if the grid-box surface area is not accounted for (crosses)

(see "Methods" section), and the colour coding of the data points refers to their chronology. The data points are all from the same reanalysis and are expected to be internally consistent, even if changes in the assimilation over time can shift the model solutions in different directions. However, the distribution of the data points reveals a tendency of having two clusters, which may involve a spurious change over time due to changing input used in the data assimilation.

The close match between $\langle f_w \rangle$ and $\overline{A'_p}$ in Fig. 1 is not unexpected since it doesn't matter if the aggregation is first done for the temporal and then in the spatial dimension or vice versa. The same analysis also reveals some discrepancies if we compare the pure average grid-box values of f_w with A_p without grid-box area weighting. If we don't account for the grid-box surface area, then the wet-day frequencies at high latitudes are weighted too high and f_w at low latitudes are weighted too low, resulting a global mean wet-day frequency that is lower than the estimate accounting for the grid-box area. This result also indicates that the wet-day frequencies at high latitudes are lower than at low latitudes.

Figure 2 presents a scatter plot between the global mean precipitation intensity $\langle \mu \rangle$ and the inverse of the fractional surface area with 24-h precipitation $1/\overline{A'_p}$ aggregated on an annual basis. The data points scatter around two clusters but nevertheless indicate a connection between the global precipitation area and the global mean precipitation intensity. A regression analysis between $\langle \mu \rangle$ and $1/\overline{A'_p}$ indicates that they are connected on a statistically significant level (p-value $< 2 \times 10^{-16}$). The Pearson correlation between them is 0.86, with a 95% confidence interval spanning 0.79 to −0.91. In other words, the correlation implies that mean annual precipitation intensity is higher when the annual mean of the daily surface area fraction with precipitation ($\overline{A'_p}$) is smaller.

The two quantities $\langle \mu \rangle$ and $\overline{P}/\overline{A'_p}$ were derived in different ways, as explained in "Methods" section, and since we also expect that $\langle \mu \rangle = \overline{P}/\overline{A'_p}$, we plotted $\langle \mu \rangle$ against $\overline{P}/\overline{A'_p}$ in Fig. 3. The results indicate a strong connection between the two sides of the equation (correlation: 0.98), albeit with a systematic bias with higher estimates of annual $\overline{P}/\overline{A'_p}$ in the ERA5 data. An ordinary linear regression analysis gave a best fit with $\langle \mu \rangle = 0.53 + 0.78\overline{P}/\overline{A'_p}$, which is not quite consistent with the expression $\langle \mu \rangle = \overline{P}/\overline{A_p}$. In this case, P had been estimated for both wet and dry days whereas days with less than 1 mm/day had been excluded in the estimation of $\langle \mu \rangle$. Hence the two quantities in this case were not exactly the same. A global sum of precipitation estimated only for grid-boxes with more than 1 mm/day also gave a high correlation, but had a different bias when comparing $\overline{P_{wet}}/\overline{A'_p}$ with $\langle \mu \rangle$ (not shown).

Figure 4 shows a scatter plot with the annual and global mean temperature anomaly $\overline{T}$ along the x-axis and the surface area fraction with precipitation (threshold 1 $\mathrm{mm/day}$) along the y-axis. The grey dashed line shows a best-fit according to an ordinary linear regression. The data points show a high correlation (−0.78) and a statistically significant dependency according to the regression analysis, implying that one degree global warming is associated with reduction in the global surface area A_p with daily precipitation by −9.7 million square km (−4.5%/K).

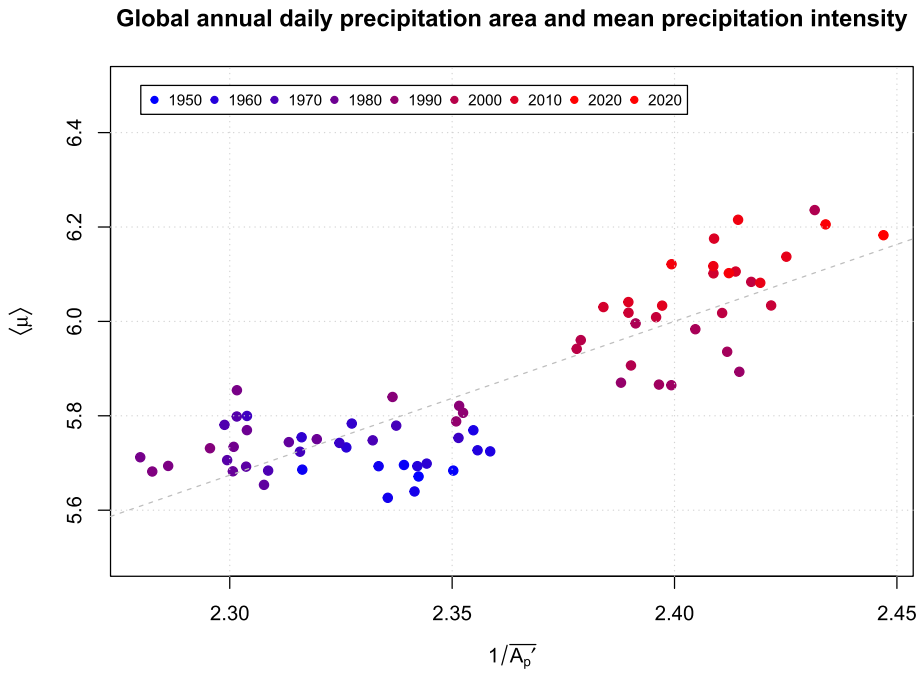

Fig. 2 The global mean precipitation intensity $\langle\mu\rangle$ shows a dependency on the fractional surface area with daily precipitation, here shown as $1/\overline{A'_p}$. Dashed grey line shows a best-fit based on ordinary linear regression with $y = -1.8 + 3.3x$, with a p-value $< 2 \times 10^{-16}$ and a correlation of 0.86 (95% confidence interval: 0.79 to − 0.91)

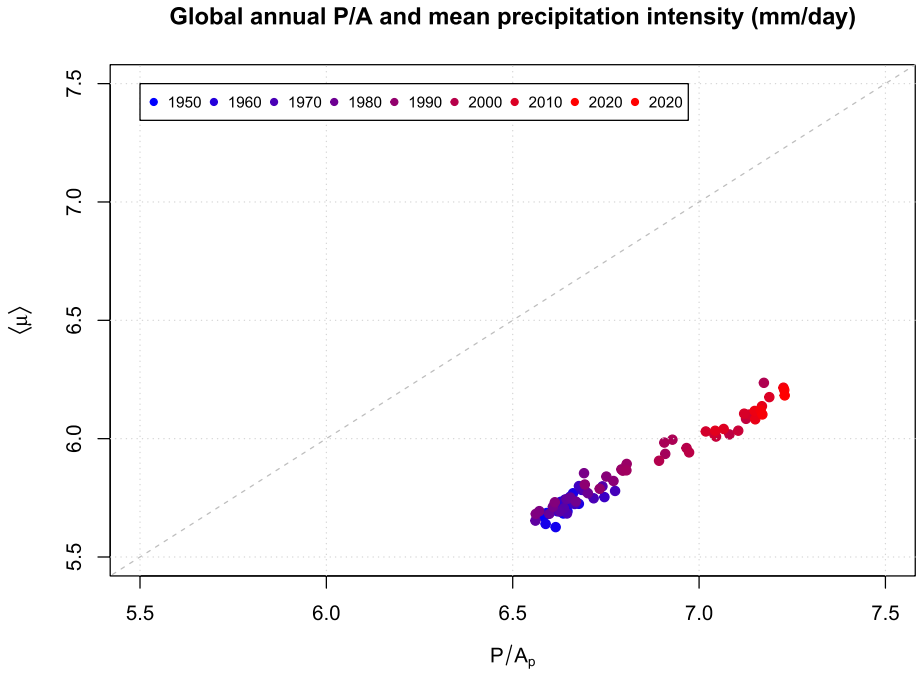

Fig. 3 There is a close relationship between the global mean precipitation intensity estimated through temporal aggregation and P/A'_p, albeit with a constant bias. Dashed grey line shows the expected one-to-one relationship and an ordinary linear regression with $\langle\mu\rangle = 0.53 + 0.78P/A'_p$ mm/day, with a p-value $< 2 \times 10^{-16}$ for the slope estimate and a correlation of 0.98 (95% confidence interval: 0.97 to − 0.99)

Figure 5 shows a similar analysis as Fig. 4, but for the annual mean of total daily mass of H_2O falling on Earth's surface in terms of percentages of the reference period 1991–2020. In this case, we repeated the analysis described in [5], comparing the percentage of total global precipitation with the global mean temperature. These results too indicated a strong relationship between the total precipitation mass and T, and the ordinary linear regression gave 62 gigatons/K (4 %/K or 0.1 mm/day per K) increase in the typical global mass of daily precipitation for each degree global warming for present global climatic conditions. We refer to the total mass here, as well as mm/day and percentage change, as the mass of water is proportional to the heat loss through latent heat of evaporation for H_2O.

A change in global mean temperature is expected to have an effect on the precipitation intensity $\langle\mu\rangle = \overline{P}/\overline{A_p}$, as both P and A_p depend on T according to the analysis presented in Figs. 4, 5. The change in $\langle\mu\rangle$ linked to a one-degree global

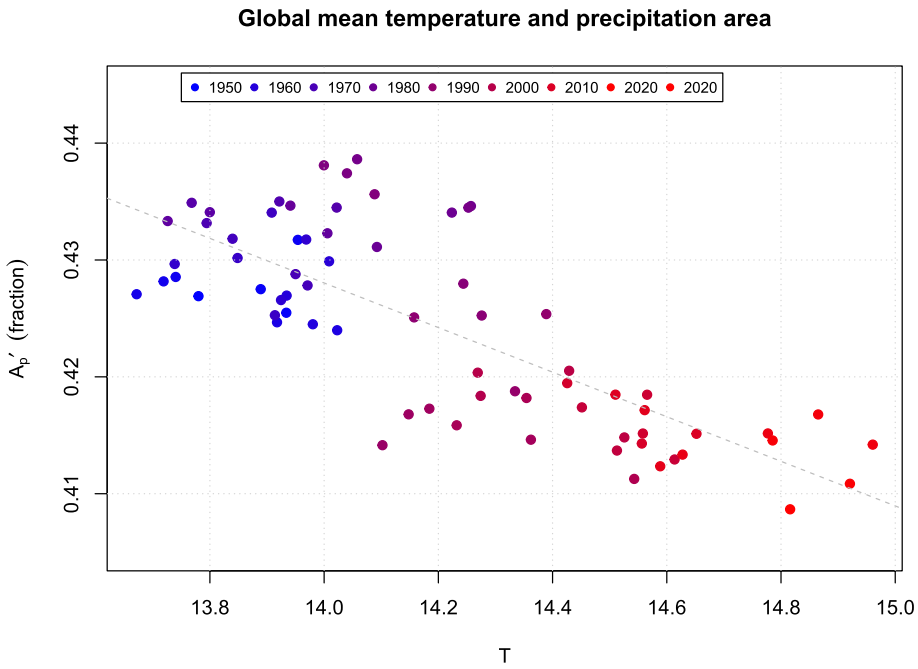

Fig. 4 There is a close connection between the fractional surface area with daily precipitation $\overline{A'_p}$ and the global mean surface temperature T, where the fractional area decreases with higher temperature. Dashed grey line shows a best-fit based on ordinary linear regression with $A'_p = 0.70 - 0.02T$, with a p-value $= 2 \times 10^{-15}$ and a correlation of -0.78 (95% confidence interval: -0.85 to -0.66)

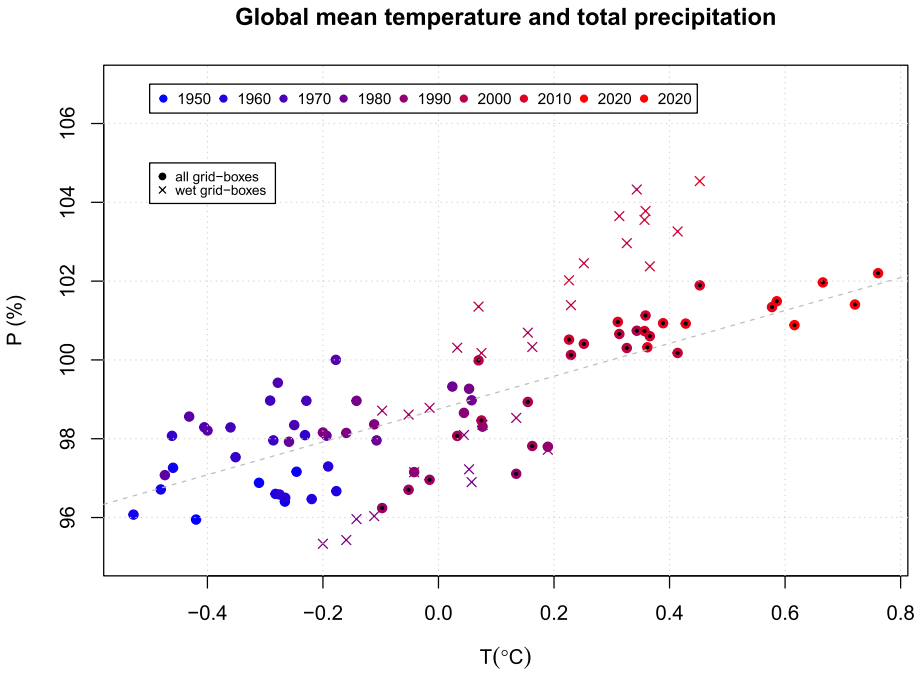

Fig. 5 The global total precipitation mass P is dependent on the global mean surface temperature anomaly T, as expected through changed rate of evaporation (Clausius–Clapeyron). Dashed grey line shows a best-fit based on ordinary linear regression with $P = 98.7 + 4.2\Delta T$ [$\Delta P = 62T$ (units: gigatons); $\Delta P = 0.1\Delta T$ (units: mm/day)], with a p-value $< 2.0 \times 10^{-16}$ and a correlation of 0.82 (95% confidence interval: 0.73–0.89). The global mean precipitation for 'wet' grid-boxes with more than 1 mm/day precipitation $\langle P_{wet} \rangle$ is also shown (crosses)

warming was estimated to be 0.47 mm/day (8%/K) and was based on an expression for a derivation product rule that included both P and A_p (see "Methods" section). Based on this derivation and the mean precipitation over the period 1950–2020, we estimated that 48.2% of the change in $\langle \mu \rangle$ could be attributed to a change in P and 51.8% to a change in A_p. In other words, the effect of a global warming on the precipitation intensity can be explained in terms of both changing thermodynamics as well as dynamical changes involving a reduction in A_p that are about equally important.

These results suggest that both μ and f_w respond to changes in the global mean temperature through changes in A_p and P. They may be representative for real-world precipitation if the precipitation simulated by ERA5 provide a good representation of measurements from rain gauges (see supporting material for details).

3 Methods

We can express the total precipitation falling on Earth's surface in terms of the average precipitation and Earth's surface area according to the expression $P = \int_A p\, dA = \langle p \rangle A$, where $\langle p \rangle$ is the spatial average of the 24-h precipitation falling on Earth. Since there are regions with zero 24-h precipitation on a daily basis, it is also possible to relate the amount of 24-h precipitation falling on Earth to the area on which it falls, A_p, and its mean intensity over this area $\int_A p\, dA = A_p \langle \mu \rangle$, where $\langle \mu \rangle$ is the average daily precipitation amount only aggregated over the surface area with 24-h precipitation A_p, or the mean precipitation intensity for 'wet' (with 1 mm/day or more) grid-boxes in the ERA5 reanalysis estimated over space.

The precipitation area is the sum of the area of the wet grid-boxes: $A_p = \sum_{i=1}^{n} \mathcal{H}(p_i - p_0) a_i$ where $\mathcal{H}$ is the Heaviside function, a_i is the area of grid-box i and n is the number of grid-boxes. The threshold p_0 for a 'wet day' was in our case set to 1 mm/day, and all parameters presented here were estimated for each grid-box of the ERA5 reanalysis [8, 9] and used as a basis for analysing the spatial distributions of f_w and μ respectively, aggregated on an annual basis. The mean precipitation intensity $\langle \mu \rangle$ was estimated by taking the area-weighted average over all grid-boxes: $\langle \mu \rangle = 1/A_p \sum_{i=1}^{n} a_i \mu_i$, where μ_i is the wet-day mean precipitation for grid-box i. The global sum of total precipitation was estimated $P = \sum_{i=1}^{n} a_i p_i$ for both wet and dry grid-boxes. The data period was 1940–2022.

We also derived local statistics aggregated over time, such as the local mean precipitation intensity μ (also referred to as the *wet-day mean precipitation*), the wet-day frequency f_w, and $\overline{p}$ which is the average of local precipitation p over time. The subscript p_t is used for a random variable at time t so that the mean precipitation and the mean precipitation intensity are related according to $\overline{p} = (1/n) \sum_{t=1}^{n} p_t = (n_w/n)\left(\sum_{t=1}^{n} p_t\right)/n_w = f_w \mu$, where n_w is the number of wet days, n is the total number of days with observations, $\mu = \sum_{t=1}^{n} p_t / n_w$, and $f_w = n_w/n$. Hence the mean precipitation amount is the product between the wet-day frequency f_w and the wet-day mean precipitation μ.

We used a ordinary linear regression (OLR) analysis to estimate best-fit coefficients for the equations $P = P_0 + \alpha T + \eta$ (expressing the precipitation in terms of percentages [5]) and $A_p = A_0 + \beta T + \zeta$, where T is the global mean temperature anomaly, whereas η and ζ are noise terms. Because the mean precipitation intensity was expected to depend on both the precipitation area and total precipitation according to $\langle \mu \rangle = \langle \mu_0 \rangle + \lambda P/A_p$, we used the analyses presented in Fig. 3 (taking the bias into account) and Fig. 4, as both P and A_p were found to be sensitive to a 1K global warming. Hence, we explored the effect of ΔT on $\langle \mu \rangle$ for the present climate based on the expression:

$$\begin{aligned} \frac{d\langle \mu \rangle}{dT} &= \lambda \frac{d(P/A_p)}{dT} \\ &= \lambda \left(\frac{1}{A_p} \frac{dP}{dT} - \frac{P}{A_p^2} \frac{dA_p}{dT} \right) \\ &= \frac{\lambda}{A_p} \left(\alpha - \frac{P\beta}{A_p} \right), \end{aligned} \tag{2}$$

where $\lambda = 0.78$ (from Fig. 3), $\alpha = \frac{dP_{glob}}{dT} = 0.122$ (in units of mm/day from Fig. 5) and $\beta = \frac{dA_p}{dT} = -0.019$ (from Fig. 4) are the slope estimates from ordinary linear regression analyses. Equation 2 is a standard mathematical differentiation following the product rule, and was used to estimate the fractional contribution of increased total global precipitation and change in surface area, due to a one degree global warming from present state, to an increase in $\langle \mu \rangle$.

The analysis presented here was carried out in the R-environment [10] and all the necessary data and method are provided as an R-markdown script in the supplementary material (https://doi.org/10.6084/m9.figshare.23735619.v2), in addition to a PDF-file with the output of the analysis. Hence, the supporting material provides complete transparency for this analysis and the results presented here

4 Discussion

A review of previous studies reveals comprehensive knowledge about Earth's global hydrological cycle with fast and slow responses in precipitation [5]. Such a review also reveals missing knowledge, such as the implication of the fractional surface area receiving precipitation on a daily basis [6]. Furthermore, advances in our understanding tend to delve into further details and increasingly complex processes, however, it's also useful to synthesise our understanding into simple

conceptual models, based on state-of-the-art data. This paper tries to provide a simple and representative heuristic description of how a global warming is connected to precipitation statistics.

The ERA5 reanalysis data reveals a link between the global surface area receiving daily precipitation A_p and the wet-day frequency $\langle f_w \rangle$ as well as the global mean precipitation intensity $\langle \mu \rangle$. Additional analysis of the data (supporting material) also suggest that the fraction of surface area with heavy precipitation (exceeding 20 mm/day and 50 mm/day) also has increased between 1940 and 2020 in a consistent way with the results obtained for $\langle f_w \rangle$ and $\langle \mu \rangle$ which can be interpreted as parameters that indicate a shift in the global statistics of local precipitation.

With the established relationships between the global hydro-climatological indicators P and A_p and statistical parameters describing the distribution for local precipitation, as well as the global mean temperature T, we can provide a crude rule-of-thumb estimate for the effect of 1K global warming ΔT on statistical parameters such as μ and f_w in terms of a change in the fractional surface area receiving daily precipitation and a change in the total mass of H_2O falling on Earth's surface. For example, a back-of-the-envelope calculation of the probability of receiving more than 30 mm/day for an 'average' situation, based on Eq. 1, estimates that a one-degree global warming changes $Pr(X > 30\,\mathrm{mm/day})$ from 0.25 to 0.32% if we use the global averages $\langle \mu \rangle$ and $\langle f_w \rangle$. These results also reveal a connection between space and time through the way A_p is linked with $\langle f_w \rangle$, and our results suggest that P/A_p corresponds well with the global mean of local $\langle \mu \rangle$ aggregated over time. In other words, time and space appear to be linked when it comes to daily precipitation statistics.

One caveat of this analysis is its reliance on just one reanalysis, in this case ERA5. A comparison between annually aggregated precipitation statistics derived from Norwegian rain gauges and corresponding quantities derived from ERA5 data interpolated to same locations gave a correlation of 0.87 for μ and 0.80 for f_w (supporting material). A recent evaluation of ERA5 over the Alps, the Carpathians and Fennoscandia, using high-quality regional datasets derived from dense rain-gauge data from these European sub-regions as reference, also has shown that ERA5 agrees qualitatively well with the reference datasets and that major mesoscale patterns in the climatology (mean, wet-day frequency, 95% quantile) are reproduced [11]. Moreover, Lavers et al. evaluated the ERA5 precipitation on a global scale and concluded that ERA5 precipitation is a better proxy for observed precipitation in extra-tropical areas than in the Tropics, though visual inspection of precipitation patterns from ERA5 and the observations broadly agrees for the extreme events they have studied [12]. Hence, the ERA5 data appear to give a representative picture of the annual rainfall statistics over Europe at least, and the results derived here can be interpreted as having some validity in terms of Earth's global hydrological cycle.

Data from the Tropical Rain Measurement mission (TRMM) suggest that the typical daily precipitation area A_p between 50° S and 50° N decreased over the period 1998–2016 [13], and a similar analysis on a global basis based on ERA5 reanalysis data also found a downward trend in the surface area receiving daily precipitation [6]. Furthermore, the analysis of the ERA5 data suggested that the reduction in surface area receiving 24-h precipitation mainly took place within the 50° S and 50° N latitude band [6]. There is a caveat with satellite and reanalysis data that potentially may lead to misleading long-term trends due to the introduction of new observational inputs over time, e.g. connected with the launch of new satellite missions. Nevertheless, there are multiple lines of evidence indicating that the surface area with daily precipitation has been shrinking over time while the total precipitation amount has increased [6, 14].

Both P and A_p turn out to be important global climate indicators, but have traditionally not been included in global sets of indicators within the meteorological community, and are not included in those currently provided by either the WMO GCOS[1] or Copernicus C3S.[2] Both are straight-forward to compute when we have reanalyses such as ERA5, and the demonstration provided here suggest they are linked to extreme rainfall amounts. Furthermore, both f_w and A_p influence the degree of dryness and aridness, and may potentially be linked to droughts [14] although this aspect is beyond the scope of present analysis. There are also some indications that μ and f_w may be linked to sub-daily amounts, e.g. through intensity–duration–frequency (IDF) curves.

The Clausius–Clapeyron equation predicts a 7% increase in water vapour for a +1K increase in temperature, however, the regression analysis herein gave a slope estimate of 4% for the increase in total precipitation amount due to a +1K global warming. According to the sixth assessment report of the IPCC [2], increases in global mean precipitation are a robust response to global surface temperature that very likely is within the range of 2–3%/K. The discrepancy between the estimates from our regression analysis and those published previously may indicate a presence of inhomogeneities in ERA5 or be sensitive to the analysed time period, such as those reported by Lavers et al. [12] and Douville et al. [15], that also may explain the two clusters of data points seen in Fig. 2. Hence, there is a caveat with these results that may

[1] https://gcos.wmo.int/en/global-climate-indicators.
[2] https://climate.copernicus.eu/climate-indicators.

be related to a potentially spurious step changes in A_p between 1980 and 1990 and after 2015 [6]. This caveat may affect the trend in A_p presented here and its dependency on the global mean temperature.

An increased rate of atmospheric overturning with more vertical displacement, which we can brand as a '*dynamic effect*' of a global warming on the hydrological cycle, implies changes in the cloud structure and rainfall patterns as well as changes in A_p. This notion is supported by the observations of higher cloud tops [16] and a deeper atmosphere and may be connected with the fast precipitation response [5]. Higher cloud tops with a deeper vertical cloud structure also favour more intense rainfall since the raindrops fall over a longer vertical distance where they can collect moisture and smaller cloud drops [17]. There have also been suggested other explanations for changes in extreme rainfall amounts, as Ombadi et al. proposed that the rainfall extremes in high-elevation regions of the Northern Hemisphere have increased by 15% per degree K of warming, double the rate expected from increases in atmospheric water vapour, which they attributed to a warming-induced shift from snow to rain [18]. Another factor may be a slow-down in storm movement, which means that the same spot receives more of the precipitation that otherwise would have been spread over a larger area [19]. None of these mechanisms exclude each other and all may be valid in different settings and locations.

5 Conclusion

Based on the ERA5 reanalysis, we demonstrate that both the daily total global amount of precipitation (P) and the part of Earth's surface area on which 24-h precipitation falls (A_p), contribute to the global mean precipitation intensity $\langle \mu \rangle$ and frequency $\langle f_w \rangle$. These statistical parameters describe the shape of the statistical distribution of local mean precipitation intensity and frequency, and a general shift in their distribution towards greater values can explain some of the increased frequency of heavy precipitation events. We estimated that a one-degree warming from present climate corresponds to an increase in the global mean precipitation intensity $\langle \mu \rangle$ by 0.47 mm/day through an ordinary linear regression analysis, for which changes in P contributes to about half of the increase and changes in A_p to the other half. Hence, both global total mass of precipitation P and the global surface area A_p are connected to the probability of heavy daily rainfall amounts. These results highlight the importance of including both the daily total global amount of precipitation and the fractional of Earth's surface area with 24-h precipitation in the list of essential global climate indicators.

Acknowledgements ERA5. Frost.

Author contributions REB carried out the analysis. CL and AD helped writing and reviewing the manuscript.

Funding The Norwegian Meteorological Institute.

Data availability See supporting material and FigShare (https://doi.org/10.6084/m9.figshare.23735619.v1).

Code availability See supporting material and FigShare https://doi.org/10.6084/m9.figshare.23735619.v2.

Declarations

Ethics approval and consent to participate Not applicable.

Consent for publication Not applicable.

Competing interests The authors declare no competing interests.

References

1. Field CB, Barros V, Stocker TF, Qin D, Dokken DJ, Ebi KL, Mastrandrea MD, Mach KJ, Plattner G-K, Allen SK, Tignor M, Midgley PM, editors. Managing the risks of extreme events and disasters to advance climate change adaptation. A special report of working groups I and II of the intergovernmental panel on climate change. Cambridge: Cambridge University Press; 2012.
2. IPCC. Climate change 2021: the physical science basis. Contribution of working group I to the sixth assessment report of the intergovernmental panel on climate change. Technical report. Cambridge: Cambridge University Press; 2021.
3. Romps DM. Clausius–Clapeyron scaling of CAPE from analytical solutions to RCE. J Atmos Sci. 2016;73(9):3719–37. https://doi.org/10.1175/JAS-D-15-0327.1.
4. Fujibe F. Clausius–Clapeyron-like relationship in multidecadal changes of extreme short-term precipitation and temperature in Japan: multidecadal changes of extreme precipitation and temperature in Japan. Atmos Sci Lett. 2013;14(3):127–32. https://doi.org/10.1002/asl2.428.
5. Allan RP, Barlow M, Byrne MP, Cherchi A, Douville H, Fowler HJ, Gan TY, Pendergrass AG, Rosenfeld D, Swann ALS, Wilcox LJ, Zolina O. Advances in understanding large-scale responses of the water cycle to climate change. Ann N Y Acad Sci. 2020;1472(1):49–75. https://doi.org/10.1111/nyas.14337.
6. Benestad RE, Lussana C, Lutz J, Dobler A, Landgren O, Haugen JE, Mezghani A, Casati B, Parding KM. Global hydro-climatological indicators and changes in the global hydrological cycle and rainfall patterns. PLOS Clim. 2022;1(5):0000029. https://doi.org/10.1371/journal.pclm.0000029.
7. Benestad RE, Parding KM, Erlandsen HB, Mezghani A. A simple equation to study changes in rainfall statistics. Environ Res Lett. 2019;14(8):084017. https://doi.org/10.1088/1748-9326/ab2bb2.
8. Hersbach H, Dee D. ERA5 reanalysis is in production. ECMWF Newsl. 2016;147. Reading: ECMWF. www.ecmwf.int/sites/default/files/elibrary/2016/16299newsletterno147spring2016.pdf.
9. Hersbach H, Bell B, Berrisford P, Hirahara S, Horanyi A, Munoz-Sabater J, Nicolas J, Peubey C, Radu R, Schepers D, Simmons A, Soci C, Abdalla S, Abellan X, Balsamo G, Bechtold P, Biavati G, Bidlot J, Bonavita M, Chiara G, Dahlgren P, Dee D, Diamantakis M, Dragani R, Flemming J, Forbes R, Fuentes M, Geer A, Haimberger L, Healy S, Hogan RJ, Holm E, Janiskova M, Keeley S, Laloyaux P, Lopez P, Lupu C, Radnoti G, Rosnay P, Rozum I, Vamborg F, Villaume S, Thepaut J. The ERA5 global reanalysis. Q J R Meteorol Soc. 2020;146(730):1999–2049. https://doi.org/10.1002/qj.3803.
10. R Core Team. R: a language and environment for statistical computing. Vienna: R Foundation for Statistical Computing; 2020. http://www.r-project.org/index.html.
11. Bandhauer M, Isotta F, Lakatos M, Lussana C, Båserud L, Izsák B, Szentes O, Tveito OE, Frei C. Evaluation of daily precipitation analyses in E-OBS (v19.0e) and ERA5 by comparison to regional high-resolution datasets in European regions. Int J Climatol. 2022;42(2):727–47. https://doi.org/10.1002/joc.7269.
12. Lavers DA, Simmons A, Vamborg F, Rodwell MJ. An evaluation of ERA5 precipitation for climate monitoring. Q J R Meteorol Soc. 2022;148(748):3152–65. https://doi.org/10.1002/qj.4351.
13. Benestad RE. Implications of a decrease in the precipitation area for the past and the future. Environ Res Lett. 2018;13(4): 044022. https://doi.org/10.1088/1748-9326/aab375.
14. Huang J, Yu H, Guan X, Wang G, Guo R. Accelerated dryland expansion under climate change. Nat Clim Change. 2016;6(2):166–71. https://doi.org/10.1038/nclimate2837.
15. Douville H, Qasmi S, Ribes A, Bock O. Global warming at near-constant tropospheric relative humidity is supported by observations. Commun Earth Environ. 2022;3(1):237. https://doi.org/10.1038/s43247-022-00561-z.
16. Norris JR, Allen RJ, Evan AT, Zelinka MD, O'Dell CW, Klein SA. Evidence for climate change in the satellite cloud record. Nature. 2016;536(7614):72–5. https://doi.org/10.1038/nature18273.
17. Rogers RR, Yau MK. A short course in cloud physics. 3rd ed. Oxford: Pergamon Press; 1989.
18. Ombadi M, Risser MD, Rhoades AM, Varadharajan C. A warming-induced reduction in snow fraction amplifies rainfall extremes. Nature. 2023;619(7969):305–10. https://doi.org/10.1038/s41586-023-06092-7.
19. Kahraman A, Kendon EJ, Chan SC, Fowler HJ. Quasi-stationary intense rainstorms spread across Europe under climate change. Geophys Res Lett. 2021. https://doi.org/10.1029/2020GL092361.